REPORT DOCUMENTATION PAGE

Form Approved
OMB No. 0704-0188

1. REPORT DATE *(DD-MM-YYYY)*	**2. REPORT TYPE**	**3. DATES COVERED** *(From - To)*
16-09-2005	Conference Paper Preprint	2005

4. TITLE AND SUBTITLE
Spacecraft Trajectory Estimation Using a Sampled-Data Extended Kalman Filter with Range-Only Measurements

5a. CONTRACT NUMBER

5b. GRANT NUMBER

5c. PROGRAM ELEMENT NUMBER

6. AUTHOR(S)
R. Scott Erwin*, Dennis S. Bernstein

5d. PROJECT NUMBER

5e. TASK NUMBER

5f. WORK UNIT NUMBER

7. PERFORMING ORGANIZATION NAME(S) AND ADDRESS(ES) AND ADDRESS(ES)
*Air Force Research Laboratory
Space Vehicles
3550 Aberdeen Ave SE
Kirtland AFB, NM 87117-5776

Dept of Aerospace Engineering
University of Michigan
Ann Arbor, MI 48109-2140

8. PERFORMING ORGANIZATION REPORT NUMBER

9. SPONSORING / MONITORING AGENCY NAME(S) AND ADDRESS(ES)
Air Force Research Laboratory
Space Vehicles
3550 Aberdeen Ave SE
Kirtland AFB, NM 87117-5776

10. SPONSOR/MONITOR'S ACRONYM(S)
AFRL/VSSV

11. SPONSOR/MONITOR'S REPORT NUMBER(S)

12. DISTRIBUTION / AVAILABILITY STATEMENT
Approved for public release; distribution is unlimited.

13. SUPPLEMENTARY NOTES
Submitted to 2006 American Control Conference, Minneapolis, MN.
Government Purpose Rights

14. ABSTRACT
Determining the trajectory of a body orbiting the Earth is a fundamental task in astrodynamics. In this paper we use a sampled-data extended Kalman Filter to estimate the trajectory of a target satellite when only range measurements are available from a constellation of orbiting spacecraft. We consider the ability of the filter to acquire the target satellite under time-sparse measurements, and to estimate the eccentricity and inclination of the target satellite's orbit. Our goal is to quantify tradeoffs among acquisition time, tracking accuracy, and measurement sample rate. In addition, when the orbits of the observing spacecraft are all equatorial, it is found that inclination maneuvers of the target satellite are unobservable.

15. SUBJECT TERMS
Astrodynamics; Space Vehicles; Trajectory; Target Satellite; Orbit; Spacecraft

16. SECURITY CLASSIFICATION OF:			**17. LIMITATION OF ABSTRACT**	**18. NUMBER OF PAGES**	**19a. NAME OF RESPONSIBLE PERSON**
a. REPORT	**b. ABSTRACT**	**c. THIS PAGE**			R. Scott Erwin
Unclassified	Unclassified	Unclassified	Unlimited	8	**19b. TELEPHONE NUMBER** *(include area code)* 505-846-9816

Standard Form 298 (Rev. 8-98)
Prescribed by ANSI Std. 239.18

Spacecraft Trajectory Estimation Using a Sampled-Data Extended Kalman Filter with Range-Only Measurements

R. Scott Erwin and Dennis S. Bernstein

Abstract— **Determining the trajectory of a body orbiting the Earth is a fundamental task in astrodynamics. In this paper we use a sampled-data extended Kalman filter to estimate the trajectory of a target satellite when only range measurements are available from a constellation of orbiting spacecraft. We consider the ability of the filter to acquire the target satellite under time-sparse measurements, and to estimate the eccentricity and inclination of the target satellite's orbit. Our goal is to quantify tradeoffs among acquisition time, tracking accuracy, and measurement sample rate. In addition, when the orbits of the observing spacecraft are all equatorial, it is found that inclination maneuvers of the target satellite are unobservable.**

1. INTRODUCTION

The problem of estimating the full state of a dynamical system based on limited measurements is of extreme importance in many applications. For the case of a linear system with known dynamics, the classical Kalman filter provides an optimal solution [1, 2]. However, state estimation for nonlinear systems remains a problem of intense research interest.

Besides their value in estimating the state of a system with nonlinear dynamics, nonlinear estimators can also be used to estimate constant states that represent parameters. Consequently, nonlinear filters are useful for system identification [3]. One of the key issues that arises in this application is parameter bias, a longstanding problem [4].

Optimal nonlinear filters have been studied [5], but are often infinite dimensional and thus are difficult to implement. Within a deterministic setting, nonlinear observers have been developed for systems of special structure [6, 7]. Consequently, except for systems of special structure, approximate filters are usually implemented in practice.

There are two main approaches to approximate nonlinear filtering. The first approach is based on a linearization of the nonlinear dynamics and measurement mapping. For example, the extended Kalman filter uses the nonlinear dynamics to propagate the state estimate while using the linearized dynamics and linearized output map to propagate the pseudo-error covariance. The extended Kalman filter is often highly effective, and documented applications cover an extraordinarily broad range of disciplines, from motor control to weather forecasting [8, 9].

Although the extended Kalman filter was originally conceived within a stochastic setting, recent research has provided a foundation for viewing the extended Kalman filter as a deterministic observer [10–12]. The idea is to adopt or modify the formalisms of the extended Kalman filter while determining conditions that ensure stability and convergence. Although the sufficient conditions are often conservative for specific applications, these results provide an intellectual rationalization for the extended Kalman filter formalism

The second approach to approximate nonlinear state estimation foregoes an explicit update of the state estimate error covariance in favor of a collection of filters whose response is used to approximate the state estimate error covariance. These statistical approaches include the particle, unscented, and ensemble Kalman filters [13–15].

The present paper is concerned with state estimation for satellite trajectory estimation, which, for unforced motion, is equivalent to orbit determination [16]. Since orbital dynamics are nonlinear, nonlinear estimation techniques are needed. A wide variety of problems can be considered based on the type of data that are available, including angle (azimuth and elevation), range, and range rate. The use of angle-only data is considered in [17], which develops a specialized filter to exploit the monotonicity of angles in orbital motion. Issues that arise in the use of range-rate (doppler) measurements are discussed in [18, 19].

Orbit estimation with measurements provided by a constellation of satellites is considered in [20, 21]. One scenario (TDRSS) considers the use of observing satellites in circular, equatorial, geosynchronous orbits to track satellites in low-Earth orbit, while another scenario (GPS) involves the use of a constellation of satellites with pseudo-range measurements (range measurements with clock error biases) to determine the location of the user.

In the present paper we consider the use of a constellation of satellites in low-Earth orbit to track a satellite in geosynchronous orbit. Since the observing satellites have much smaller period than the target satellite in geosynchronous orbit, we must account for blockage by the Earth, and thus the number of available measurements varies with time. We are particularly interested in the ability of the observing satellites to acquire and track the target satellite

R. Scott Erwin is with the Air Force Research Lab, Space Vehicles Directorate, Kirtland Air Force Base, NM, richard.erwin@kirtland.af.mil

Dennis S. Bernstein is with the Department of Aerospace Engineering, The University of Michigan, Ann Arbor, MI 48109-2140, dsbaero@umich.edu

when measurements are available at low frequency, that is, with a large sample interval.

Unlike the study in [20, 21], which considers either angle (two observations per satellite), angle and range (three observations per satellite), and angle, range, and range rate (four observations per satellite), we consider the case in which only range measurements are available (one observation per satellite). In addition, the sample rate in [20] was chosen to be 33 Hz, while we are interested in the ability to track under time-sparse measurements, available on a scale of only minutes or perhaps hours. This constraint is motivated by the need for satellites to simultaneously track a large number of objects.

As in [20, 21], we employ the sampled-data (continuous-discrete) extended Kalman filter [2, p. 188]. This extended Kalman filter involves continuous-time propagation of the state estimate as well as the pseudo-error covariance between measurements and data updates. In practice, the continuous-time state and covariance propagation can be implemented online with high-resolution integration to accurately follow the nonlinear dynamics.

2. Equations of Motion

We consider a single body, called the *target*, orbiting the Earth. Throughout this study we assume that the Earth is spherical and uniform with an ideal gravitational field. Except for possible thrusting by the target itself, we ignore all perturbing forces such as drag. The position vector $\vec{r}$ of the target with respect to the center of the Earth satisfies

$$\ddot{\vec{r}} = \frac{-\mu}{r^3}\vec{r} + \vec{w}, \tag{1}$$

where $r \triangleq |\vec{r}|$ is the distance from the satellite to the center of the Earth, $\vec{w}$ denotes forces due to thrusting per unit mass acting on the target, and $\mu \triangleq 398,600$ km^3/s^2 is the Earth's gravitational parameter. The specific thrust $\vec{w}$ is zero unless the target is actively maneuvering. Introducing the velocity vector $\vec{v} \triangleq \dot{\vec{r}}$, we can rewrite (1) as

$$\dot{\vec{r}} = \vec{v}, \tag{2}$$

$$\dot{\vec{v}} = \frac{-\mu}{r^3}\vec{r} + \vec{w}. \tag{3}$$

To cast the dynamics (3) in terms of coordinates, we introduce an inertial reference frame I. It is traditional to choose the inertial reference frame so that the X-axis points toward the Sun on the first day of spring (the vernal equinox line), the Z-axis points through the North pole of the Earth along the axis of rotation, and the Y-axis completes a right-handed coordinate system. This description is approximate since the Earth's rotational axis is not fixed inertially and since the stars move inertially as well [22, pp. 150–153]. However, such details do not play a role in the subsequent analysis.

Resolving $\vec{r}$, $\vec{v}$, and $\vec{w}$ in I according to

$$\vec{r}\Big|_{\mathrm{I}} = \begin{bmatrix} x \\ y \\ z \end{bmatrix}, \vec{v}\Big|_{\mathrm{I}} = \begin{bmatrix} v_x \\ v_y \\ v_z \end{bmatrix}, \vec{w}\Big|_{\mathrm{I}} = \begin{bmatrix} w_x \\ w_y \\ w_z \end{bmatrix},$$

the equations of motion (3) become

$$\begin{bmatrix} \dot{x} \\ \dot{y} \\ \dot{z} \\ \dot{v}_x \\ \dot{v}_y \\ \dot{v}_z \end{bmatrix} = \begin{bmatrix} v_x \\ v_y \\ v_z \\ -(\mu/r^3)x + w_x \\ -(\mu/r^3)y + w_y \\ -(\mu/r^3)z + w_z \end{bmatrix}. \tag{4}$$

Note that $r = \sqrt{x^2 + y^2 + z^2}$. We can rewrite (4) as

$$\dot{X} = f(X) + W, \tag{5}$$

where

$$X \triangleq \begin{bmatrix} x \\ y \\ z \\ v_x \\ v_y \\ v_z \end{bmatrix}, f(X) \triangleq \begin{bmatrix} v_x \\ v_y \\ v_z \\ -(\mu/r^3)x \\ -(\mu/r^3)y \\ -(\mu/r^3)z \end{bmatrix}, W \triangleq \begin{bmatrix} 0 \\ 0 \\ 0 \\ w_x \\ w_y \\ w_z \end{bmatrix}. \tag{6}$$

The vector X provides a complete representation of the target's state, which is characterized by the position and velocity. When the satellite is moving along an orbit, such as a circle, ellipse, parabola, or hyperbola, it is often useful to represent the satellite motion in terms of the 6 orbital parameters given by the perigee distance r_{p}, the eccentricity e, the right ascension of the ascending node Ω, the inclination i, the argument of periapsis ω, and the true anomaly ν. The orbital elements r_{p} and e fix the shape of the orbit, while the angles Ω, i, and ω comprise a $(3, 1, 3)$ sequence of Euler rotations that transform the inertial frame to the inertially fixed frame. The true anomaly $\nu(t)$ is a time-dependent parameter that keeps track of the position of the satellite along its orbit. The nonlinear transformations that convert position and velocity into orbital elements and vice versa are given in [22].

3. Measurement Model

For trajectory estimation, we assume that range measurements are available from p satellites at times $t = kh$, where $k = 1, 2, \ldots$. Letting x_i, y_i, z_i denote the inertial coordinates of the ith satellite, assumed to be known accurately, the measurement $Y = Y(kh) \in \mathbb{R}^p$ is given by (omitting the argument kh on the right-hand side)

$$Y(kh) = \begin{bmatrix} d_1(x, y, z, x_1, y_1, z_1) \\ \vdots \\ d_p(x, y, z, x_p, y_p, z_p) \end{bmatrix} + v, \tag{7}$$

where, for $i = 1, \ldots, p$,

$$d_i(x, y, z, x_i, y_i, z_i) \triangleq [(x - x_i)^2 + (y - y_i)^2 + (z - z_i)^2]^{1/2} \tag{8}$$

is the distance from the ith satellite to the target, and $v \in \mathbb{R}^p$ denotes measurement noise.

The measurement d_i is assumed to be unavailable when the line-of-sight path between the ith satellite and the target is blocked by the Earth. To determine blockage, we note that the Earth's surface blocks the path from the ith satellite to the target if and only if there exists $\alpha \in [0,1]$ such that $D_i(\alpha) < R_{\mathrm{E}}$, where $R_{\mathrm{E}} \triangleq 6378$ km is the radius of the Earth and

$$D_i(\alpha) \triangleq \sqrt{(x_i + \alpha x)^2 + (y_i + \alpha y)^2 + (z_i + \alpha z)^2}.$$

The smallest value of $D_i(\alpha)$ as attained for $\alpha = \alpha_i$, where

$$\alpha_i \triangleq -\frac{x_i x + y_i y + z_i z}{x^2 + y^2 + z^2}.$$

Hence, we compute α_i, ascertain whether α_i lies in the interval $[0,1]$, and then check the blockage condition $D_i(\alpha_i) < R_{\mathrm{E}}$.

4. Sampled-Data Extended Kalman Filter

Since the equations of motion (1) are nonlinear, we consider an extended Kalman filter. In addition, since we assume that measurements Y are available with a specified sample interval of h sec, we consider a sampled-data extended Kalman filter with data update performed at each time $t = kh$. The sampled-data ("continuous-discrete") extended Kalman filter is given in [2, p. 188]. We use "-" and "+" to denote state estimates before and after data updates, respectively.

4.1. Forecast Step

The forecast (data-free) step of the sampled-data extended Kalman filter consists of the state-estimate propagation

$$\dot{\hat{X}}(t) = f(\hat{X}(t)), \quad t \in [(k-1)h, kh], \tag{9}$$

where

$$\hat{X} \triangleq \begin{bmatrix} \hat{x} & \hat{y} & \hat{z} & \hat{v}_x & \hat{v}_y & \hat{v}_z \end{bmatrix}^{\mathrm{T}}, \tag{10}$$

as well as the pseudo-error covariance propagation

$$\dot{P}(t) = \hat{A}(t)P(t) + P(t)\hat{A}^{\mathrm{T}}(t) + Q, \quad t \in [(k-1)h, kh], \tag{11}$$

where $\hat{A}(t) \triangleq f'(\hat{X}(t))$ is the Jacobian of f evaluated along the trajectory of (9). The Jacobian $\hat{A}(t)$ is given by

$$\hat{A}(t) = \begin{bmatrix} 0_{3\times 3} & I_3 \\ \hat{A}_0(t) & 0_{3\times 3} \end{bmatrix},$$

where (omitting the argument t)

$$A_0(t) \triangleq \mu \begin{bmatrix} \frac{3\hat{x}^2}{\hat{r}^5} - \frac{1}{\hat{r}^3} & \frac{3\hat{x}\hat{y}}{\hat{r}^5} & \frac{3\hat{x}\hat{z}}{\hat{r}^5} \\ \frac{3\hat{x}\hat{y}}{\hat{r}^5} & \frac{3\hat{y}^2}{\hat{r}^5} - \frac{1}{\hat{r}^3} & \frac{3\hat{y}\hat{z}}{\hat{r}^5} \\ \frac{3\hat{x}\hat{z}}{\hat{r}^5} & \frac{3\hat{y}\hat{z}}{\hat{r}^5} & \frac{3\hat{z}^2}{\hat{r}^5} - \frac{1}{\hat{r}^3} \end{bmatrix},$$

where $\hat{r} \triangleq \sqrt{\hat{x}^2 + \hat{y}^2 + \hat{z}^2}$.

Equations (9) and (11) are numerically integrated in real time. Since there is no data injection during the time interval $[(k-1)h, kh]$, variable-step integration can be used for efficiency and accuracy. Let $\hat{X}(kh-)$ and $P(kh-)$ denote the values of $\hat{X}$ and P at the right-hand endpoint of the interval $[(k-1)h, kh]$. At the start of the next interval $[kh, (k+1)h]$, the initial values $\hat{X}(kh+)$ and $P(kh+)$ are determined by the data update step. The overall system can be viewed as a sampled-data system in which continuous-time dynamics are interrupted by instantaneous state jumps [23].

4.2. Data Update Step

For the data update step, the linearized measurement map is given by

$$\hat{C}_k \triangleq \begin{bmatrix} \frac{\hat{x}(kh-)-x_1(kh)}{\hat{d}_1(k)} & \frac{\hat{y}(kh-)-y_1(kh)}{\hat{d}_1(k)} & \frac{\hat{z}(kh-)-z_1(kh)}{\hat{d}_1(k)} & 0_{1\times 3} \\ \vdots & \vdots & \vdots & \vdots \\ \frac{\hat{x}(kh-)-x_p(kh)}{\hat{d}_p(k)} & \frac{\hat{y}(kh-)-y_p(kh)}{\hat{d}_p(k)} & \frac{\hat{z}(kh-)-z_p(kh)}{\hat{d}_p(k)} & 0_{1\times 3} \end{bmatrix},$$

where, for $i = 1, \ldots, p$,

$$\hat{d}_i(k) \triangleq d_i(\hat{x}(kh-), \hat{y}(kh-), \hat{z}(kh-), x_i(kh), y_i(kh), z_i(kh)).$$

Furthermore, the data update gain K_k is given by

$$K_k = P(kh-)\hat{C}_k^{\mathrm{T}}[\hat{C}_k P(kh-)\hat{C}_k^{\mathrm{T}} + R]^{-1}, \tag{12}$$

while the state-estimate data update is given by

$$\hat{X}(kh+) = \hat{X}(kh-) + K_k[Y(kh) - \hat{d}(k)], \tag{13}$$

where

$$\hat{d}(k) \triangleq \begin{bmatrix} \hat{d}_1(k) \\ \vdots \\ \hat{d}_p(k) \end{bmatrix}.$$

Finally,

$$P(kh+) = (I - K_k\hat{C}_k)P(kh-).$$

The values $\hat{X}(kh+)$ and $P(kh+)$ are used to initialize (9), (11) in the next interval $[kh, (k+1)h]$.

5. Numerical Examples

We consider the case in which satellites in low-Earth orbit (LEO) at a radius of 6600 km are observing a target satellite in an equatorial geosynchronous orbit at a radius of 42,164 km. We assume that the LEO satellites are spaced uniformly around the Earth in an equatorial orbit. With this arrangement, 4 is the smallest number of satellites for which at least 2 satellites are always able to simultaneously view the target. Target tracking with as few as 2 satellites separated by a true anomaly of less than 180 degrees is also possible as long as measurements are guaranteed to be available when the target is in the field of view of both satellites. However, for simplicity, we assume the availability of 4 uniformly spaced LEO satellites with range

measurements available (subject to blocking by the Earth) at a fixed sample interval of h sec. All satellite measurements (blocked or not) are assumed to occur simultaneously.

Assuming perfect knowledge of the initial condition and assuming that the target is not maneuvering, it is possible to track the target with arbitrary accuracy without the use of measurements. In practice, perturbing forces such as drag must also be estimated; however, these forces are not considered in this study. When the initial state is unknown or when the target is maneuvering, measurements are needed to track the target. We consider these cases separately.

6. Target Acquisition

We first consider the ability of the sampled-data Kalman filter to acquire the target, that is, to locate the target despite initial position errors. In all cases we set $Q = \left[\begin{smallmatrix} 0 & 0 \\ 0 & I_3 \end{smallmatrix}\right]$, and $P_0 = 0$.

First, we set the sample interval to be $h = 1$ sec, and we consider initial estimates that are erroneous by 1 degree and 110 degrees. We assume perfect (nonnoisy) measurements and set $R = 0.01I$ in (12). Figure 1 compares the performance of the filter for both initial estimates. The ultimate tracking accuracy in both cases is determined by numerical resolution in computing the state estimates. Convergence of the filter is not global; in fact, the filter fails to converge for initial true anomaly errors greater than about 120 degrees.

Next, we introduce gaussian measurement noise with a standard deviation of 0.1 km, which corresponds to $R = 0.01I$ in (12). For initial estimates that are erroneous by 1 degree and 110 degrees, Figure 2 shows that the position-estimate error reaches a level that is consistent with the measurement accuracy.

For an initial true anomaly estimate that is erroneous by 110 degrees, the position estimates are shown in Figure 3. The estimator approaches the vicinity of the target within about 10 sec.

Next we consider the ability of the filter to acquire the target under time-sparse measurements with a measurement standard deviation of 0.1 km. For an initial true anomaly error of 10 degrees, Figure 4 shows the position-estimate errors for $h = 1, 10, 50, 100$ sec. In each case, the estimator acquires the target in about 10 data assimilation steps, with ultimate accuracy independent of the sample interval.

7. Intermeasurement Tracking Accuracy

Next, we assess the ability of the filter to track the target along its orbit. To see how the position estimate degrades between data updates, we consider an initial true anomaly error of 10 degrees and a sample interval of 50 sec with measurement noise having a standard deviation of 0.1 km. Figure 5 shows the growth of the position error between measurements as well as the position-error reduction that occurs due to data injection.

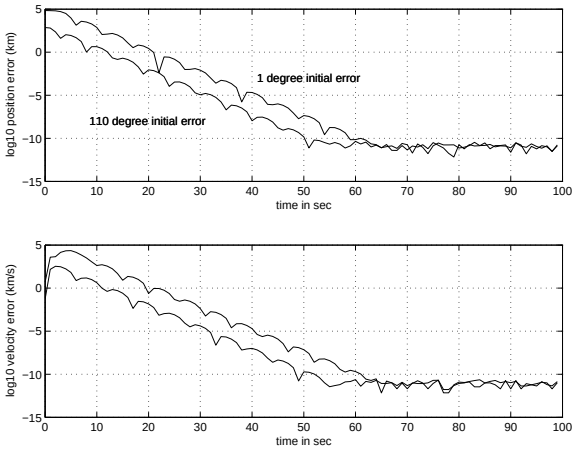

Fig. 1. Target position- and velocity-estimate errors with initial true anomaly errors of 1 degree and 110 degrees. The range data are measured with a sample interval $h = 1$ sec from 4 LEO satellites, and perfect (nonnoisy) measurements are assumed with $R = 0.01I$ in the filter gain expression (12). In both cases the estimator accurately locates the target within about 50 sec.

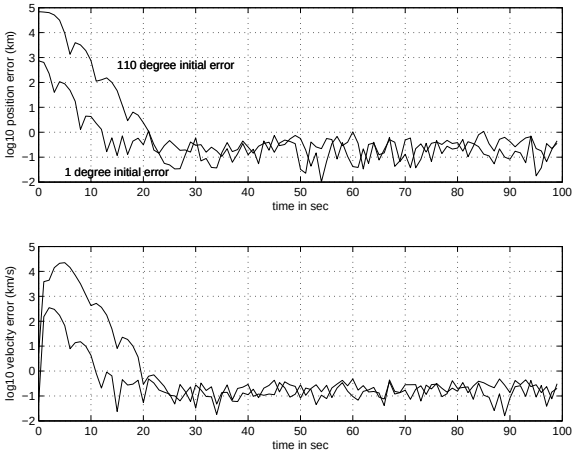

Fig. 2. Target position- and velocity-estimate errors with initial true anomaly errors of 1 degree and 110 degrees. The range data are measured with a sample interval $h = 1$ sec from 4 LEO satellites, and with gaussian measurement noise whose standard deviation is 0.1 km and thus with $R = 0.01I$ in the filter gain expression (12). In both cases the estimator accuracy corresponds to the measurement error level.

8. Eccentricity Estimation

We now consider the case in which the target performs an unknown thrust maneuver that changes the eccentricity of its orbit. The initial true anomaly error in all cases is 10 degrees. In particular, the target is initially in a circular orbit as in the previous examples. At time $t = 100$ sec, the target performs a 1-second burn that produces a specific thrust $w = [0\ .5\ 0]^{\mathrm{T}}$ km/s^2, and, at time $t = 200$ sec, the target performs a 1-second burn that produces a specific thrust $w = [0\ .3\ 0]^{\mathrm{T}}$ km/s^2. With an initial eccentricity of $e = 0$, corresponding to the initial circular orbit, the eccentricity after the first burn is $e \approx .35$, while the eccentricity after the second burn is $e \approx .59$. Assuming measurement noise

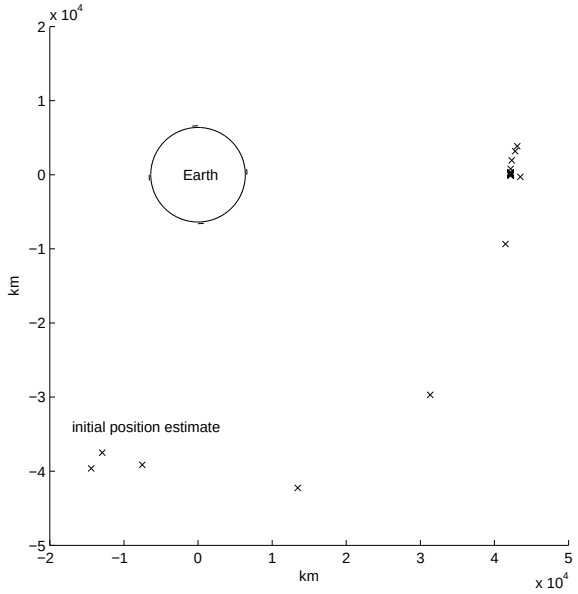

Fig. 3. Target position estimates '×' with an initial true anomaly error of 110 degrees. The initial location of the target is at 3:00. The range data are measured with a sample interval $h = 1$ sec from 4 LEO satellites (whose tracks are shown), and with gaussian measurement noise whose standard deviation is 0.1 km and thus with $R = 0.01I$ in the filter gain expression (12). The estimator approaches the vicinity of the target within about 10 sec. The Earth and all orbit locations are drawn to scale.

with a standard deviation of 0.01 km and measurements available with a sample interval of $h = 1$ sec, the estimated eccentricity based on the data update estimates is shown in Figure 6. The same scenario is repeated with h increased to 10 sec, with the results shown in Figure 7.

9. Inclination Estimation

We now consider the case in which the target performs an unknown thrust maneuver that changes its inclination. The initial true anomaly error in all cases except where noted is 30 degrees. In particular, the target is initially in a circular equatorial orbit as in the previous examples. At time $t = 100$ sec, the target performs a 1-second burn that produces a specific thrust $w = [0\ 0\ .5]^{\mathrm{T}}$ km/s^2, and, at time $t = 200$ sec, the target performs a 1-second burn that produces a specific thrust $w = [0\ 0\ -.2]^{\mathrm{T}}$ km/s^2. With an initial inclination of $i = 0$ rad, corresponding to the initial equatorial orbit, the inclination after the first burn is $i \approx 0.16$ rad, while the inclination after the second burn is $i \approx 0.097$ rad. Assuming measurement noise with a standard deviation of 0.01 km, the estimated inclination based on the data update estimates is shown in Figure 8.

Figure 8 shows that, after a transient, the filter correctly converges to the target's inclination of 0 rad. However, the filter fails to detect the changes in inclination due to the target's maneuvers. This failure suggests that the out-plane-maneuver is due to a lack of observability by the observing satellites. In fact, the numerical rank of the observability matrix formed from $(\hat{A}(kh-), \hat{C}_k)$ is found to be 4.

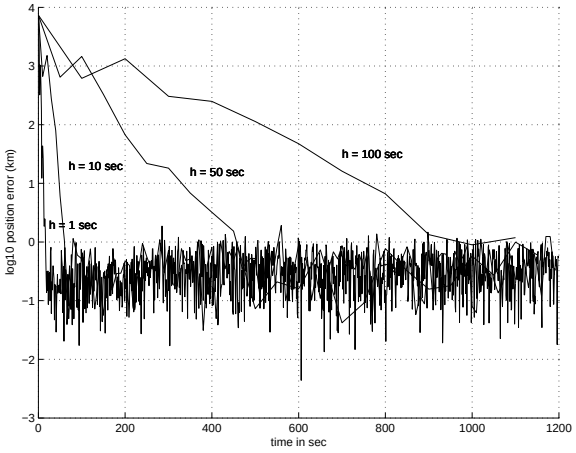

Fig. 4. Target position-estimate error for sample intervals $h = 1, 20, 50, 100$ with range data measured from 4 LEO satellites with a standard deviation of 0.1 km. In each case, the estimator acquires the target in about 10 data assimilation steps, with ultimate accuracy independent of the sample interval.

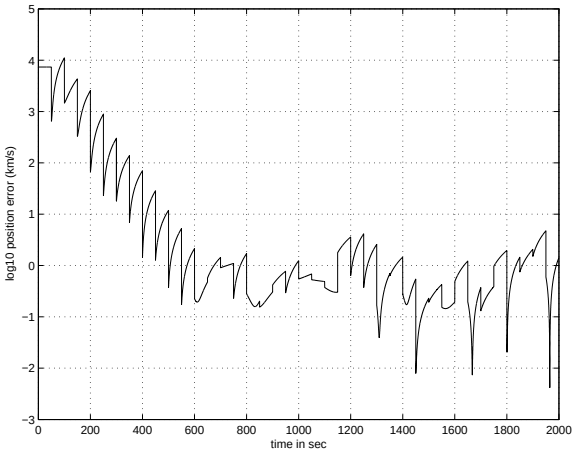

Fig. 5. Target position-estimate error with an initial true anomaly error of 10 degrees, a sample interval of $h = 50$ sec, and a measurement noise standard deviation of 0.1 km. The growth of the position error between measurements can be seen, as well as the position-error reduction that occurs due to data injection.

Next, we slightly change the orbit of the first observing satellite by giving it an inclination of -0.1 rad. Figure 9 shows a strong transient that prevents the filter from estimating the initial 0 rad inclination despite the fact that the initial inclination estimate is correct, followed by a noisy estimate of the inclination after the first burn, followed, finally, by a biased estimate of the inclination after the second burn.

Next, we also change the orbit of the second observing satellite by giving it an inclination -0.2 rad. After an initial transient, Figure 10 shows an improved ability to estimate the true inclination.

Finally, we increase the sample interval to $h = 10$ sec. In this case, the filter diverges. However, for an initial true anomaly error of 5 degrees, it can be seen from Figure 11

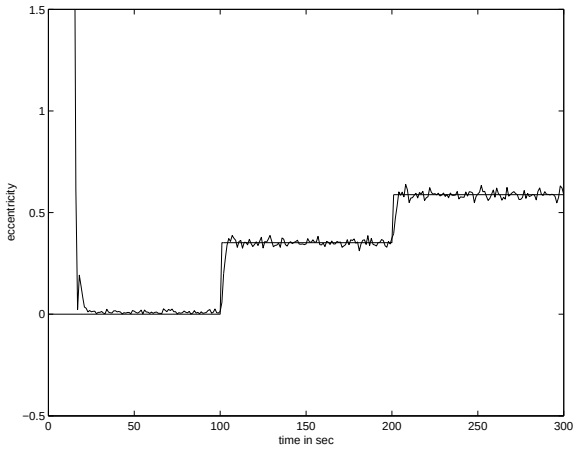

Fig. 6. Estimated eccentricity. The target performs unknown 1-second burns at $t = 100$ sec and $t = 200$ sec. The initial eccentricity is $e = 0$, corresponding to the initial circular orbit, while the eccentricity after the first burn is $e \approx .35$, and the eccentricity after the second burn is $e \approx .59$. Assuming a 1-second measurement interval and measurement noise with a standard deviation of 0.01 km, the estimated eccentricity follows the true eccentricity. The apparent bias for the initial eccentricity $e = 0$ is an artifact of the constraint $e \geq 0$. The full extent of the initial estimate transient is not shown.

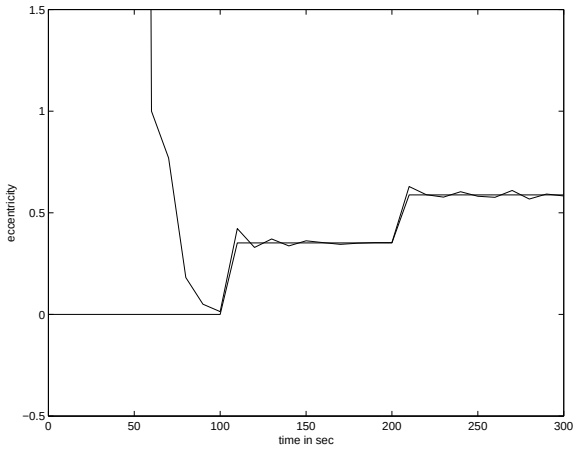

Fig. 7. Estimated eccentricity. This simulation is analogous to Figure 6, where now the sample interval is $h = 10$ sec. Again, the full extent of the initial estimate transient is not shown.

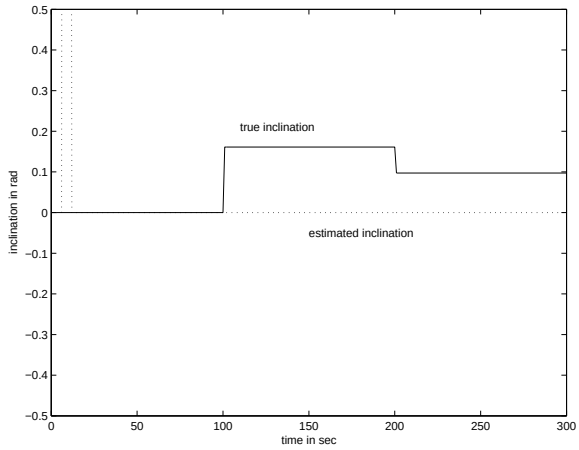

Fig. 8. Estimated inclination. Although the filter correctly converges to the target's initial inclination of 0 rad, the filter fails to detect the changes in inclination due to the target's maneuvers. Numerical tests suggest a lack of observability by the observing satellites.

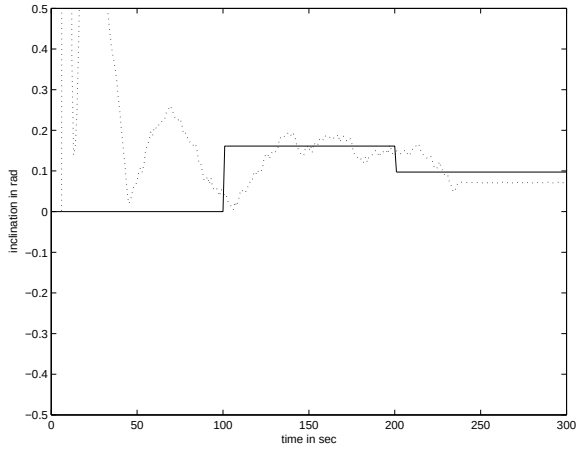

Fig. 9. Estimated inclination. In this case, the orbit of the first observing satellite by given an inclination of -0.1 rad. A strong transient prevents the filter from estimating the initial 0 rad inclination despite the fact that the initial inclination estimate is correct. The estimate of the inclination after the first maneuver is noisy, while the estimate of the inclination after the second burn is biased.

that the filter can detect changes in the target's inclination.

10. Concluding Remarks

Under idealized assumptions on the astrodynamics of bodies orbiting the Earth, we developed a sampled-data Kalman filter for range-only observations provided by a constellation of 4 low-Earth orbiting satellites in circular, equatorial, geosynchronous orbits. We studied the ability of the filter to acquire and track a target satellite in geosynchronous orbit as a function of the sample interval, initial true anomaly error, and measurement noise standard deviation.

This study complements previous studies that have considered combinations of angle, range, and range-rate measurements by considering range measurements alone and by considering the effects of infrequent measurements.

A surprising discovery of our study is the apparent inability of a constellation of 4 LEO satellites to track a maneuvering target satellite that changes its inclination. Naive numerical tests based on linear time-invariant notions suggest that the dynamics of the target satellite are unobservable using the available measurements. Therefore, future research will seek to apply nonlinear observability tests [24–26] to better understand how observability of the target's dynamics depends on the geometry of the observing constellation and the types of available measurements.

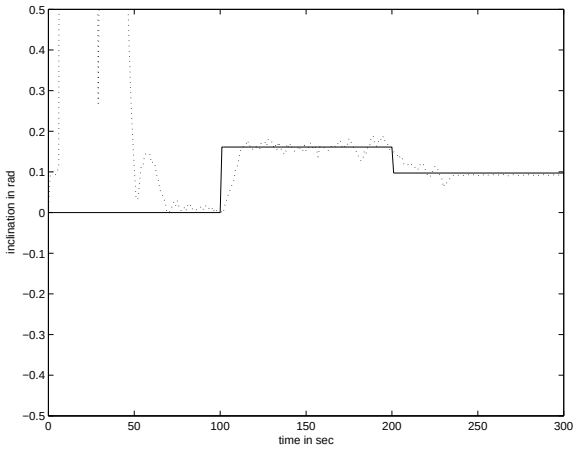

Fig. 10. Estimated inclination. In addition to the inclination of the orbit of the first observing satellite, the second observing satellite is given an inclination of -0.2 rad. After an initial transient, the filter provides improved estimates of the target's inclination.

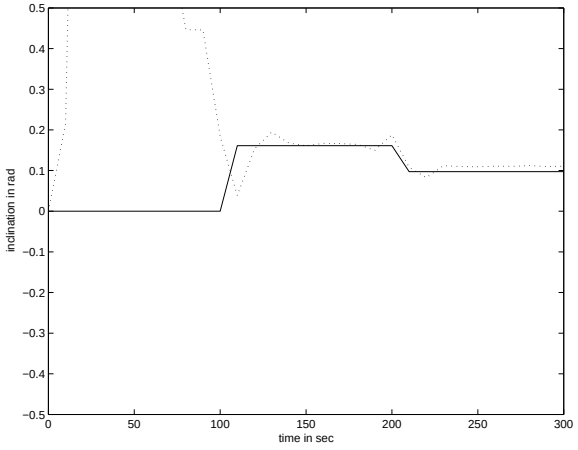

Fig. 11. Estimated inclination. In addition to the inclinations of the orbits of the first and second observing satellites, the sample interval is increased to $h = 10$ sec. Despite this constraint, the filter retains the ability to detect changes in the target's inclination.

REFERENCES

[1] A. H. Jazwinski, *Stochastic Processes and Filtering Theory*, Academic Press, 1970.

[2] A. Gelb, Ed., *Applied Optimal Estimation*, MIT Press, Cambridge, 1974.

[3] S. K. Sinha and T. Nagaraja, "Extended Kalman Filter Algorithm for Continuous System Parameter Identification," *Comput. Elec. Eng.*, vol. 16, pp. 51–64, 1990.

[4] L. Ljung, "Asymptotic Behavior of the Extneded Kalman Filter as a Parameter Estimator for Linear Systems," *IEEE Trans. Autom. Contr.*, vol. AC-24, pp. 36–50, 1979.

[5] F. E. Daum, "Exact Finite-Dimensional Nonlinear Filters," *IEEE Trans. Autom. Contr.*, vol. 31, pp. 616–622, 1986.

[6] A. J. Krener and W. Respondek, "Nonlinear Observers with Linearizable Error dynamics," *SIAM J. Contr. Optim.*, vol. 23, pp. 197–216, 1985.

[7] P. E. Moraal and J. W. Grizzle, "Observer Design for Nonlinear Systems with Discrete-Time Measurements," *IEEE Trans. Autom. Contr.*, vol. 40, pp. , 1995.

[8] S. Bolognani, L. Tubiana, and M. Zigliotto, "Extended Kalman Filter Tuning in Sensorless PMSM Drives," *IEEE Trans. Ind. Appl.*, vol. 39, pp. 1741–1747, 2003.

[9] S. Carme, D.-T. Pham, and J. Verron, "Improving the Singular Evolutive Extended Kalman Filter for Strongly Nonlinear Models for Use in Ocean Data Assimilation," *Inverse Problems*, vol. 17, pp. 1535-1559, 2001.

[10] Y. Song and J. W. Grizzle, "Extended Kalman Filter as a Local Asymptotic Observer for Discrete-time Nonlinear Systems," *J. Math. Sys. Estim. Contr.*, vol. 5, pp. 59–70, 1995.

[11] M. Boutayeb, H. Rafaralahy, and M. Darouach, "Convergence Analysis of the Extended Kalman Filter Used as an Observer for Nonlinear Deterministic Discrete-time Systems," *IEEE Trans. Autom Contr.*, vol. 42, pp. 581–586, 1997.

[12] K. Reif, Konrad and R. Unbehauen, "Extended Kalman Filter as an Exponential Observer for Nonlinear Systems," IEEE Trans. Sig. Proc., vol. 47, pp. 2324–2328, 1999.

[13] S. Julier, J. Uhlmann, and H. F. Durrant-Whyte, "A New Method for the Nonlinear Transformation of Means and Covariances in Filters and Estimators," *IEEE Trans. Autom. Contr.*, vol. 45, pp. 477–482, 2000.

[14] F. E. Daum, "Beyond Kalman Filters: Practical Design of Nonlinear Filters," *Proc. SPIE Int. Soc. Opt. Eng.*, vol. 2561, pp. 252–262, 1995.

[15] P. L. Houtekamer and H. L. Mitchell, "Data Assimilation Using an Ensemble Kalman Filter Technique," *Monthly Weather Review*, vol. 126, pp. 796-811, 1998.

[16] B. D. Tapley, B. E. Schutz, and G. H. Born, *Statistical Orbit Determination*, Elsevier, Amsterdam, 2004.

[17] J. L. Fowler and J. S. Lee, "Extended Kalman Filter in a Dynamic Spherical Coordinate System for Space Based Satellite Tracking," AIAA 23rd Aerospace Sciences Meeting, paper AIAA-85-0289, Reno, NV, 1985.

[18] D. E. Bizup and D. E. Brown, "Maneuver Detection Using the Radar Range Rate Measurement," *IEEE Trans. Aerosp. Elec. Sys.*, vol. 40, pp. 330–336, 2004.

[19] D. E. Bizup and D. E. Brown,"The Over-Extended Kalman Filter–Don't Use It?," preprint.

[20] D. A. Cicci and G. H. Ballard, "Sensitivity of an Extended Kalman Filter 1. Variation in the Number of Observers and Types of Observations," *Appl. Math. Comput.*, vol. 66, pp. 233–246, 1994.

[21] D. A. Cicci and G. H. Ballard, "Sensitivity of an Extended Kalman Filter 2. Variation in the Observation Error Levels, Observation Rates, and Types of Observations," *Appl. Math. Comput.*, vol. 66, pp. 247–259, 1994.

[22] H. D. Curtis, *Orbital Mechanics for Engineering Students*, Elsevier, Amsterdam, 2005.

[23] W. Sun, K. Nagpal, M. Krishan, and P. Khargonekar, "Control and Filtering for Sampled-Data Systems," *IEEE Trans. Autom. Contr.*, vol. 38, pp. 1162–1175, 1993,

[24] H. Nijmeijer, "Observability of Autonomous Discrete-time Nonlinear Systems: A Geometric Approach," *Int. J. Contr.*, vol. 36, pp. 867–874, 1982.

[25] J. P. Gauthier and I. A. K. Kupka, "Observability and Observers for Nonlinear Systems," *SIAM J Contr. Optim.*, vol. 32, pp. 975-994, 1994.

[26] B. Tibken "Observability of Nonlinear Systems - An Algebraic Approach," *Proc. IEEE Conf. Dec. Contr.*, pp. 4824–4825, December 2004,